

11

Global Climate Models

11.1 MATHEMATICAL MODELING

We can better understand and predict climate and its variations by incorporating the principles of physics, chemistry, and biology into a mathematical model of climate. A climate model can range in complexity from the simple energy-balance models described in Chapter 2, whose solution can be worked out on the back of a small envelope, to very complex models that require the biggest and fastest computers and the most sophisticated numerical techniques. This chapter will discuss more complex global climate models, since these are the models that can produce the most realistic simulations of climate and are the tool on which we place our hope of predicting future climates in sufficient detail to be useful for planning purposes. These models are also useful for understanding the climate system and how various processes interact to determine the structure that climate change will take.

One can distinguish two general types of climate models at the present time. The first type specifies most of the key climate forcings and then uses a model of the physical climate system to compute the response of the climate. For brevity, we will refer to this type of model as “GCM,” which we can take to be an acronym for *global climate model*. This type of model is also sometimes called an atmosphere–ocean general circulation model (AOGCM), since the fluid motions of both the atmosphere and ocean are explicitly calculated. A hierarchy of progressively less complicated climate models exists. These less detailed models are also useful for gaining understanding. Another level of complexity beyond the GCM is the *Earth system model* (ESM), which may include elaborations way beyond the physical climate system, including the carbon cycle, soil evolution, vegetation that adapts to climate, and may even include human infrastructure and decision making as predicted variables within the model. Current ESMs include the carbon cycle to interactively predict atmospheric CO₂, and can also include chemical and biologic models to predict other

trace gases, aerosols, and cloud condensation nuclei. Models that allow the vegetation cover to react to climate change have also been developed. Most of the discussion here will focus on GCMs, rather than ESMs.

11.2 HISTORICAL DEVELOPMENT OF CLIMATE MODELS

The modern GCM has its roots in the computer models that were first developed to predict weather patterns a few days in advance. L. F. Richardson (1922) was the first to promote the idea that future weather could be predicted by numerically integrating the equations of fluid motion using the present weather as the initial condition. He attempted a hand calculation of a weather forecast while serving as an ambulance driver in France during World War I. The forecast was spectacularly inaccurate, because his initial conditions contained a large spurious wind convergence. The first successful numerical forecasts used a set of equations that are greatly simplified compared to Richardson's and for which the solution is less sensitive to the initial conditions.

Numerical weather prediction was proposed as one potential use for the electronic computer developed by John von Neumann in the late 1940s. The first successful numerical weather forecast with an electronic computer was conducted at the Institute for Advanced Study in Princeton, New Jersey (Charney et al., 1950). This model had only one atmospheric layer and described the region over the continental United States. It included only the fluid dynamical evolution of an initial velocity distribution and none of the physical processes that drive the climate. The first numerical experiment that included radiation and dissipation was conducted by Norman Phillips (1956) using a simple model with only two levels in the vertical. Later, more detailed simulations of the atmospheric general circulation included a more accurate formulation of the equations of motion, more spatial resolution in the horizontal and vertical, and more realistic specifications of the physical processes that drive the atmospheric circulation, such as radiation, latent heat release, and frictional dissipation (Smagorinsky, 1963; Manabe et al., 1965). With these and succeeding models, it has become possible to simulate the general circulation of the atmosphere with reasonable fidelity. The quality of the simulations obtained with atmospheric models has benefited greatly from intensive experimentation associated with providing practical weather forecasts, starting in 1955 with the first routine numerical weather forecasts that were conducted by the U. S. Joint Numerical Weather Prediction Unit. Associated with the practical effort to provide weather forecasts is a substantial effort to collect routine weather observations at the surface and at upper levels of the atmosphere. These observations are capable of describing the

atmospheric state in sufficient detail to justify newly initialized forecasts about every 6 h, which are able to provide some useful information about the weather more than a week in the future. The initial states for weather forecasting that are constructed by assimilating all useful observations into a numerical weather prediction model also serve as the primary tool for diagnosing and understanding the atmospheric general circulation, a key part of the climate system, as discussed in Chapter 6. A key contribution to understanding the general circulation and validating climate models has been through *reanalysis* of weather data using state-of-the-art weather models to produce the best record of the atmospheric state during the recent past (Kalnay et al., 1996; Dee et al., 2011).

Numerical models of oceanic general circulation have been constructed by applying the same basic techniques used for atmospheric models. Development of oceanic general circulation models has lagged behind atmospheric models both because the observational base is less in the ocean and because the computational problems are greater for oceanic simulations. No longstanding effort has been undertaken to observe and predict the state of the global ocean on an operational basis, so oceanographers have not had a base in numerical weather forecasting on which to build an oceanic climate modeling enterprise until very recently. Operational forecasts with oceanic initial conditions were employed to make forecasts of El Niño starting in the 1980s. An observed climatology of the ocean that is sufficiently detailed and accurate for climate purposes is still being developed, particularly for the deep ocean. The spatial scale of the significant motion systems is small compared to the width of an ocean basin, and observations of currents, temperature, and salinity at depths below the surface must be acquired from ships and are expensive. Therefore, the number of observations taken in a year has typically been less than is necessary to define the state of the ocean, until perhaps quite recently, when profiling drifting buoys have been deployed across the global ocean and satellites have measured the sea level height variations. The speed of many important ocean currents is small and therefore difficult to observe with great precision, so observing systems focus on temperature, salinity, and ocean surface height. Also, a very long integration time is necessary for an oceanic model to achieve a stable climatology. Although the atmosphere will spin up to climatology from rest in a few weeks or months, the deep circulation in the ocean requires many centuries to spin up from rest or to respond to changed conditions. This long integration time and the high spatial resolution required for realistic simulations of ocean circulation mean that numerical experimentation with ocean models can require substantial and sophisticated computer resources. The number and complexity of the physical processes required for ocean simulation are much less than in the atmosphere, but the circulation is very sensitive to mixing by tides and other processes that are not well understood or modeled.

Early simulations of the atmosphere were obtained by fixing the sea surface temperature. Similarly, early ocean general circulation models assumed fixed wind stress, air temperature, air humidity, precipitation, and radiative forcing. Together these determined the flux of momentum, heat, and freshwater at the surface, which are the key driving forces of the ocean circulation. In a fully general model of the climate, the exchanges of heat, moisture, and momentum between the ocean and the atmosphere must be internally determined so that the state of the coupled climate system can evolve in a consistent manner. Initial experiments with fully coupled atmosphere–ocean models often produced climates that were very different from reality, even though the atmosphere and ocean components each produced a reasonable climatology when run independently with realistic fixed boundary conditions. The greater freedom of fully coupled atmospheric–ocean climate models to determine their own climate has revealed many deficiencies in atmospheric and oceanic general circulation models, and these deficiencies are being addressed through current research efforts. Improved climate simulation and prediction will also require land-surface processes to be treated with greater accuracy and detail.

The schematic parts of an Earth system model are shown in Fig. 11.1. An Earth system model includes not only the physical climate system

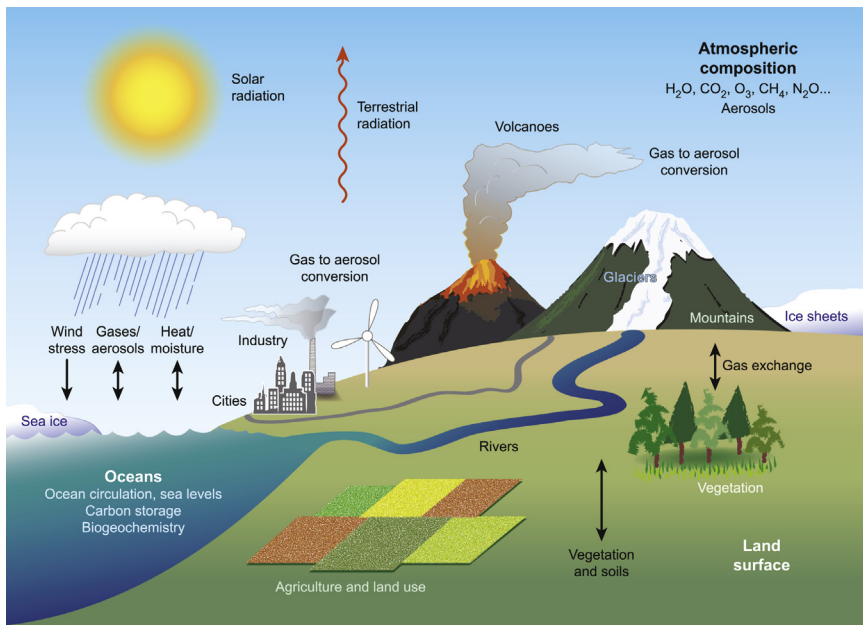


FIGURE 11.1 Schematic of the Earth system. The basic elements include the physical elements of the atmosphere, hydrosphere, cryosphere, and land surface, plus the biosphere, all of which interact strongly with humans. *Figure by Beth Tully.*

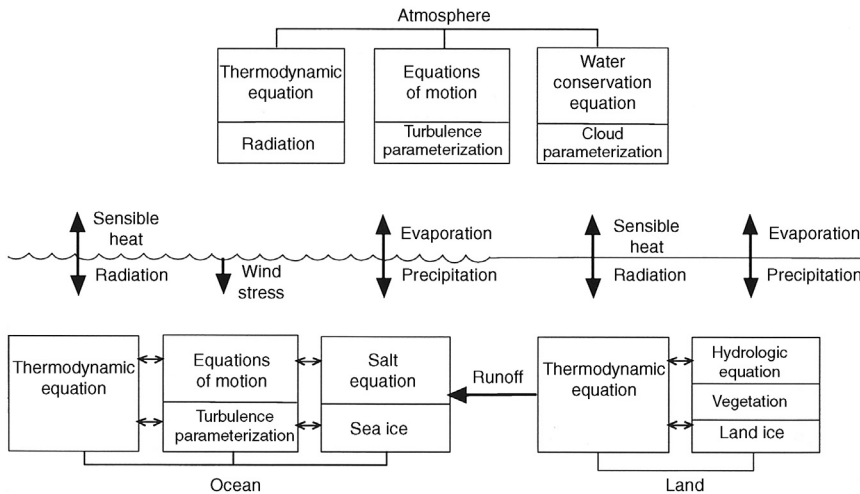


FIGURE 11.2 Schematic diagram of the physical components of a global climate model. This is divided into atmosphere, ocean, and land.

but also the biosphere and human influences, and predicts atmospheric composition, vegetation changes, and many other things not typically included in early climate models. The biogeochemical feedbacks, which determine the atmospheric composition and the nature of the land vegetation, are included. For example, increased CO₂ in the air can cause plants to open their leaf stomata less, which can affect the release of water by plants, which can in turn affect the soil moisture and temperature. These processes were not included in first-generation climate models, but are increasingly being included in Earth system models. All of the components and the processes represented within them are critical to the understanding and simulation of climate.

The component parts of a global climate model that includes only physical processes are shown schematically in Fig. 11.2. This is organized according to the three primary physical components of the climate system: the atmosphere, the ocean, and the land surface. The cryosphere is split between the oceans, where sea ice is important, and the land surface, where snow, glaciers, and ice sheets may form.

11.3 THE ATMOSPHERIC COMPONENT

The atmospheric component of a global climate model is basically the same as a model constructed for the purpose of weather forecasting. Improvements of numerical weather prediction systems have been fostered by efforts to predict weather more than a week in advance. For these

longer predictions, the similarity of the model’s “climatology” with reality is very important. The errors in the climatology of the model make a large contribution to the errors in these medium range forecasts. Efforts to make longer weather forecasts and to accurately simulate climate are thus synergistic and together are leading to improvements in atmospheric models.

The basic framework of a numerical model of the atmosphere or ocean is a spatial grid work on which the equations of physics are represented. Sometimes so-called spectral methods are used wherein the fields of velocity, temperature, and pressure are represented with continuous functions in order to efficiently solve the equations of motion. These methods allow very accurate calculation of the derivatives needed for following the flow of heat and momentum, but the fields must be interpolated to grid points in order to calculate radiative heating and the effects of sub-grid-scale processes such as convection. The globe is thus always divided into geographic regions or grid cells. The size and number of the grid cells are limited by the amount of computer power available and the time period over which the model must be integrated. Numerical weather prediction models that focus on deterministic 10-day forecasts currently use about 15 km horizontal resolution and about 150 vertical levels. Models that are run many times to make ensembles of forecasts to assess probabilities of weather events are generally run at lower resolution, but forecasts are done many times with slightly different initial conditions. Since climate models may be required to simulate decades or centuries, and include many more processes than a weather model, the spatial resolution is generally much less, currently about 100 km. The spatial resolution and the number of experiments that can be conducted are generally limited by the speed of the fastest computers, which steadily increases. Because the time step must also be reduced when the grid spacing is reduced, to increase the spatial resolution by a factor of two, say from 100 km to 50 km, requires about a factor of 10 increase in computing power.

Vertical resolution is also important to the quality of an atmospheric simulation. Climate models currently have typically about 20–50 levels. The levels are not equally spaced in height or pressure, but tend to be most closely spaced near the lower boundary and near the tropopause, where rapid changes take place and greater resolution is needed. The total number of latitude, longitude, and height grid points represented in an atmospheric model may thus be around 10 million.

11.3.1 The Conservation Equations

The basic dynamical framework of a GCM includes the solution of the equations describing the conservation of momentum, mass, and energy for a fluid. In addition, a water conservation equation for air is needed to predict the amount of water vapor in the atmosphere. Water vapor is critical for the formation of clouds and rain, and is one of the most important

variables in the calculation of radiative heating. Numerical models of the atmosphere use the equations of motion in a simplified form called the *primitive equations*. Use is made of the fact that the atmosphere is thin in comparison to its horizontal extent in order to approximate the vertical momentum balance with the hydrostatic balance. Models that do not make the hydrostatic assumption are being developed. Earth is assumed to be spherical and some other small terms in the momentum equations are neglected. If the hydrostatic balance is assumed, the vertical coordinate can be height or pressure. Since it facilitates the inclusion of topography and makes it easier to construct a numerical solution that conserves mass, the *sigma coordinate*, which is pressure normalized by surface pressure, is often used as the vertical coordinate in atmospheric primitive equation models.

The sources and sinks of momentum and heat are associated with phenomena that occur at scales that are much smaller than the grid resolution and so cannot be explicitly simulated. These are often called sub-grid-scale phenomena, and their effects must be specified from knowledge of the state of the atmosphere at the grid scale. This process of including the effect of unresolved phenomena according to the large-scale conditions is called *parameterization*.¹ Key parameterizations in atmospheric models include radiation, the effects of unresolved turbulence and gravity waves, and the effects of convection on the heat, moisture, and momentum budgets. The behavior of the climate model is critically dependent on these parameterized processes.

11.3.2 Radiation Parameterization

Radiative heating from the sun and infrared cooling to space provide the basic drive of the climate system (Chapters 2 and 3). Radiative transfer models that are incorporated in current climate models do not consider each individual absorption line but rather treat groups of lines or band systems in a statistical or empirical manner. They consider the atmosphere and the embedded clouds to be horizontally homogeneous within a grid box. Despite these simplifications, it is generally believed that the transmission of radiation, at least under clear sky conditions, is accurately treated in climate models. Although there are some discrepancies between various parameterization schemes, the basic physical processes and the methods necessary to treat them are reasonably well understood. The largest uncertainties in radiative flux calculations are associated with clouds and the manner in which the amount and nature of the clouds in the model are determined. Early general circulation models typically specified cloud radiative properties as externally

¹The word parameterization is used because one or more adjustable constants or parameters must be introduced to relate sub-grid-scale processes to large-scale conditions.

determined quantities that were often zonally invariant with a fixed seasonal variation. More recent climate models predict cloud amounts and optical properties, which can then interact with the other elements of the climate system. These newer models treat cloud microphysics in some parameterized way and carry cloud water and ice as predicted variables. The predicted cloud water and ice provide a means of connecting the water budget, radiation calculation, and heat budget in a manner that is consistent between the parameterized processes and the large-scale conservation equations.

11.3.3 Convection and Cloud Parameterization

Clouds affect radiative transfer, and the convective motions associated with clouds produce important fluxes of mass, momentum, heat, and moisture. The spatial scales at which cloud properties are determined are generally much smaller than the grid size at which the atmosphere is represented in a climate model, yet the vertical fluxes of heat and moisture associated with sub-grid-scale convection are often greater than those of the large-scale flow. The timing and intensity of precipitation in the tropics and over land areas during summer are controlled as much by unresolved mesoscale phenomena as by the large-scale flow. The atmospheric state averaged over the area of a typical climate model grid box may be stable to moist convection even when intense convection is occurring somewhere in the grid box. Cloud and convection parameterization seek to address the mismatch between the spatial resolution of climate models and the spatial scale of convective motions and clouds.

At least three important effects in a climate model are associated with the formation of clouds: (1) the condensation of water vapor and the associated release of latent heat and rain; (2) vertical transports of heat, moisture, and momentum by the motions associated with the cloud; and (3) the interaction of the cloud particles with radiation. A cloud parameterization in a climate model should treat each of these effects consistently, but this is not yet the case with every climate model. The release of latent heat during intense convection and the radiative effects of the associated clouds drive the Hadley circulation and other important components of the general circulation of the atmosphere, so that the coupling of deep convection to the large-scale flow is critical to a proper simulation of climate.

Most climate models include at least two types of clouds: convective clouds and large-scale supersaturation clouds. Large-scale supersaturation clouds occur when the relative humidity in a grid box at some model level exceeds a critical value. This can be implemented by assuming that condensation occurs in the grid box when the relative humidity reaches

some threshold like 80%. Another alternative is to assume that sub-grid-scale temperature variability occurs within the grid box and that the fraction of the grid box where the temperature variability causes the relative humidity to reach 100% is cloud covered.

Convective clouds are associated with the buoyant ascent of saturated air parcels in a conditionally unstable environment. The simplest convective parameterization is moist adiabatic adjustment. If the lapse rate exceeds the moist adiabatic lapse rate (Fig. 1.10), the moisture and heat are readjusted in a vertical layer such that the air in the layer is saturated, the lapse rate equals the moist adiabatic lapse rate, and energy is conserved. Excess moisture is assumed to rain out, but momentum is not transported. In this parameterization, the entire grid box is assumed to behave like a convective element, whereas in reality convection occurs at much smaller spatial scales. Other parameterization schemes attempt to predict the effect of an ensemble of convective cloud elements on the air properties averaged over the grid cell, so that the grid cell is only infrequently saturated or unstable. In the future, when computing power is sufficient that climate models can be run with grid resolution finer than about 1 km, it is hoped that the parameterization of convection will be unnecessary, or at least less of a strong constraint on model behavior. Since cloud properties depend so importantly on the availability of cloud condensation nuclei and ice nuclei, state-of-the-art climate models used for predicting future climates will need to include explicit modeling of the abundance and chemistry of these aerosols.

11.3.4 Planetary Boundary-Layer Parameterization

In the atmospheric boundary layer, rapidly fluctuating phenomena with vertical and horizontal space scales much smaller than the grid spacing of climate models determine the fluxes of heat, momentum, and moisture between the surface and the atmosphere. These phenomena include turbulence, gravity waves, and rolls or other coherent structures that cannot be resolved by climate models and must therefore be parameterized. The simplest and most often used parameterizations are the bulk aerodynamic formulas and similarity theories briefly described in Section 4.6. These formulas allow the boundary layer to be treated as a single layer through which the fluxes can be calculated using the mean variables resolved by the model. They can be made dependent on vertical stability and surface roughness. These models may be elaborated by adding a prediction equation for the boundary-layer depth.

If the model has sufficient resolution to have several levels within the boundary layer, then eddy diffusion formulations may be used in which the vertical eddy fluxes are assumed to be proportional to the vertical derivative of the mean for the model grid box.

$$\overline{w'T} = -K_T \frac{\partial \bar{T}}{\partial z} \quad (11.1)$$

The simplest approach is to make the flux coefficient, K_T , a constant, but more realistic parameterizations include height and stability dependencies.

Higher-order closure schemes include prognostic equations for the turbulent kinetic energy in the boundary layer and more complex equations than (11.1) for the vertical eddy fluxes. These models require more than a few computational levels in the planetary boundary layer (PBL) and carry a heavier computational burden. It can be argued that statistical closure schemes do not describe the essential physics of the coherent structures that appear to produce much of the vertical flux in the boundary layer and thereby control the response of this flux to mean conditions. In many cases, the boundary layer contains clouds, and in such cases moist processes are critical to the behavior of the boundary layer. Some planetary boundary-layer parameterizations incorporate a separate parameterization for boundary-layer clouds. Oceanic stratocumulus and trade wind cumulus clouds are important examples where the interaction of the boundary layer with low clouds is essential. In regions of deep convection, the boundary layer properties and the cloud fluxes interact very strongly, so that the PBL parameterization and the convection parameterization must be compatible. The PBL parameterization must also be compatible with the land-surface parameterizations that may incorporate the effect of plant canopies on the fluxes of momentum, heat, and moisture between the surface and the atmosphere.

11.4 THE LAND COMPONENT

The land component of a climate model must contain the surface heat balance equation (4.1) and a surface moisture equation that is at least as sophisticated as the models described in Fig. 5.7 and includes a model for snow cover. Land topography can readily be incorporated in a climate model, but the fidelity with which Earth's surface topography can be included is limited by the resolution of the model. Many important mountain ranges are much narrower than the grid spacing of a GCM, so that smoothed representations of topography must be used.

Experiments with GCMs that include these basic prescriptions for the land surface indicate a substantial climate response to the soil moisture and to the surface albedo. Low soil moisture generally results in a warmer surface and less local evaporation and rainfall. These changes are consistent with the observation that much of the precipitation in such areas as the central United States during summer and the Amazon Basin during

the rainy season is re-evaporated rainfall rather than water vapor that has been carried into the region by the atmospheric circulation. The changes in the surface fluxes of latent and sensible heat affect the thermal forcing of atmospheric flow and may thereby cause further weather and climate anomalies. Extreme events, such as the 2003 European drought have been shown to be exacerbated by preexisting dry soil (Fischer et al., 2007), and much of the interannual variability of summertime temperature over land is related to feedbacks between soil moisture and surface temperature.

In land areas, the storage of precipitation in the soil and the subsequent release of this moisture to the air are strongly dependent on the soil type and the vegetative cover. In addition, the absorption of solar radiation and the emission of longwave radiation are sensitive to the geometry and physical state of the vegetative cover. Turbulent transports of heat and moisture between the atmosphere and the soil are also affected by the physical structure of the plant canopy, particularly for forested areas. Parameterizations of surface processes that include all of these effects have been developed in recent years and are being incorporated in climate models. These parameterizations treat the vegetative cover as a variable resistance that moderates the flow of moisture from the soil to the atmosphere. Over land areas, the diurnal cycle of convection is very important, and parameterizations often initiate convection too early or too late and this affects the mean climate over land.

11.5 THE OCEAN COMPONENT

The oceanic component of a global climate model is also built on a framework of the equations of motion describing the general circulation of the ocean, although informative climate simulation experiments can also be conducted with fixed sea surface temperatures, or with an ocean model that is a simple mixed layer that stores heat and releases water vapor, but does not transport heat. Ocean general-circulation models differ from atmospheric models in that the fluid is water, rather than air, and the geometry of the ocean basins is more important and complex. The fundamental driving mechanisms for the ocean circulation include wind stress at the upper surface, radiative and sensible heat fluxes through the surface, and density variations caused by changes in salinity and temperature. Salinity changes are induced at the surface by precipitation, evaporation, runoff, salt rejection during sea ice formation, and the addition of freshwater during sea ice melting. These salinity variations are carried to the interior of the ocean by fluid motions that are forced in part by the density variations associated with salinity and heat.

The spatial resolution with which the oceanic circulation can be resolved is again limited by the computing time required to complete a simulation.

A typical model at the present time might have horizontal resolution of about 10 km with around 50 vertical levels. When you consider that critically important features such as the Gulf Stream and Kuroshio currents are less than 100 km in width, the horizontal resolution currently used in the ocean component of climate models is just at the margin of being adequate. Most models that are run for climatological purposes require parameterized diffusion to simulate the effect of eddies on the general circulation. Mixing by tidal motions and turbulence are small in the ocean, but have a very strong effect on the resulting ocean climate. In atmospheric models, the corresponding eddies are much larger in scale and can be explicitly modeled without parameterization. Ocean model runs with higher spatial resolution reveal many more details and features that are not well represented in simulations with coarser resolution. In some regions such as the Southern Ocean, resolution of transient ocean eddies is necessary to obtain a realistic ocean climate.

11.6 SEA ICE MODELS

Sea ice plays a critical role in climate by increasing the albedo of the ocean surface, inhibiting the exchanges of heat, moisture, and momentum between atmosphere and ocean, and altering the local salinity during sea ice freezing and melting. Thermodynamic processes lead to freezing and melting of seawater, and dynamic processes, such as driving by winds and currents, cause mechanical deformation and transport of sea ice. In most climate models, at least a thermodynamic model of sea ice is employed. Transport of sea ice by winds and currents is treated with varying degrees of complexity, ranging from mixed-layer ocean models with no ice transport at all, to more complete models that calculate the movement of ice in response to both winds and currents.

The simplest model predicts the thickness of a layer of sea ice based on thermodynamic considerations. When the temperature of the upper layer of the ocean reaches the freezing point of seawater (-2°C) and the surface energy fluxes continue to remove heat from the water, then surface ice is assumed to form. Heat transport through this layer of ice is assumed to be described by a flux-gradient relationship.

$$F_I = -k_I \frac{\partial T}{\partial z} \quad (11.2)$$

A layer of snow may be present on top of the sea ice through which heat is also conducted. The thermal conductivity for ice, $k_I \approx 2 \text{ W m}^{-1} \text{ K}^{-1}$, is much larger than the thermal conductivity of snow, $k_s \approx 0.3 \text{ W m}^{-1} \text{ K}^{-1}$, so that a layer of snow greatly increases the thermal insulation provided by the sea ice. Snow cover also increases the albedo. If all heat fluxes,

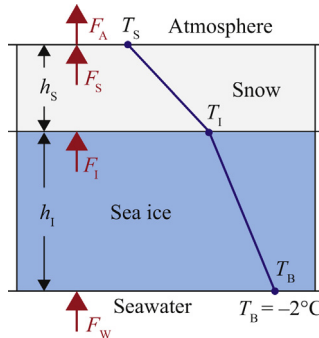


FIGURE 11.3 Schematic diagram of a simple sea ice model with a layer of snow over a layer of ice and the fluxes of heat through the layers. The temperature profiles in the two layers are linear if penetration of solar radiation is ignored and a steady state is assumed. Symbols are as defined in the text.

including solar heating, are assumed to be applied at the surface rather than distributed over some depth, then in steady state the flux through the snow and ice would be equal at every depth. Constant flux implies a linear temperature profile, so that the heat flux becomes proportional to the temperature difference across the ice layer. Under these steady conditions, the temperature profile within the layer of snow and ice would be as shown in Fig. 11.3. The fluxes across the ice and snow layers can then be written in terms of the temperature difference across the layers.

$$F_I = k_i \frac{T_B - T_i}{h_i}, \quad F_s = k_s \frac{T_i - T_s}{h_s} \quad (11.3)$$

where T_s is the surface temperature, T_B is the temperature at the base of the sea ice layer, T_i is the temperature at the interface between ice and snow, and h_i and h_s are the depth of the ice and snow layers, respectively. The interface temperature can be eliminated by applying the requirement that in a steady state the heat flux must be the same through the snow layer and the ice layer. The flux through the sea ice can then be expressed in terms of the temperature difference across the snow–ice layer and the depth of each layer.

$$F_I = \frac{k_i k_s}{k_i h_s + k_s h_i} (T_B - T_s) = \gamma_{SI} (T_B - T_s) \quad (11.4)$$

Here γ_{SI} is the combined thermal conductance of the snow–ice layer. For a thick layer $\gamma_{SI} \approx 1 \text{ W m}^{-2} \text{ K}^{-1}$, and for a thin layer $\gamma_{SI} \approx 20 \text{ W m}^{-2} \text{ K}^{-1}$. The surface temperature can be determined from the requirement that the net heat flux at the surface be zero, which is consistent with our previous

assumption of no heat storage in the ice. The net heat flux includes the conductive flux through the ice, and the latent, sensible, and net radiative heating of the surface. The depth of the snow layer is determined by the balance of snowfall, sublimation–evaporation, and melting. If no snow is present, then the ice layer may be reduced in thickness by melting and sublimation at the top. Growth of the ice layer occurs at the bottom, where it is assumed to thicken at a rate such that the heat of fusion will just balance the net heat flux at the bottom of the ice layer and thus keep the lower edge of the ice at the freezing point. Similarly, if the equilibrium surface temperature would exceed the freezing point, ice is assumed to melt at a rate sufficient to keep the temperature at the freezing point until all of the ice is melted.

Sea ice grows rapidly when it is thin and more slowly as thickness increases; when subjected to similar thermal forcing, ice a few centimeters thick grows nearly a hundred times faster than ice that is 2 or 3 m thick. The reason for this is because of the insulating effect of the ice itself. Consider a sheet of sea ice that is growing as a result of an imposed temperature difference between the ice surface and the seawater. The thickness of the sea ice increases at a rate necessary to balance the heat flux through the ice with the latent heat of fusion needed for freezing seawater at the base of the ice.

$$\rho_i L_f \frac{\partial h_i}{\partial t} = \frac{k_i}{h_i} (T_B - T_s) - F_w \quad (11.5)$$

Here ρ_i is the density of ice, L_f is the latent heat of fusion for seawater, and F_w is the rate at which heat is supplied to the sea ice by ocean fluxes. It is notable that for fixed surface temperature, the growth rate of the ice thickness is inversely proportional to the thickness itself. Integrating (11.5) over time, assuming $F_w = 0$, we find that the ice thickness is proportional to the square root of the integral over time of the temperature difference, so that the ice grows more slowly as it thickens.

$$h_i^2(t) - h_i^2(t_0) = \frac{k_i}{\rho_i L_f} \int_{t_0}^t (T_B - T_s) dt \quad (11.6)$$

[Figure 11.4](#) shows solutions to (11.5) for different values of F_w , assuming that the ice thickness is initially very thin and that $T_B = -2^\circ\text{C}$ and $T_s = -30^\circ\text{C}$. This illustrates how thin ice initially grows very quickly, then more slowly as the ice becomes thicker. [Figure 11.4](#) also shows that the equilibrium thickness of the ice is very sensitive to the amount of heat supplied by the ocean to the bottom of the sea ice. If the ocean heat flux to the bottom of the ice is large, then the sea ice equilibrates quickly to a thin layer. If the ocean heat flux is low, then the sea ice can grow slowly too much greater thickness.

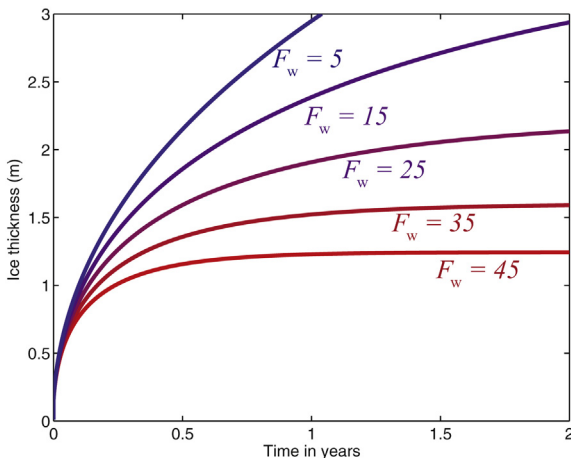


FIGURE 11.4 Plot of sea ice thickness as a function of time from the simple model (11.5) for different values of the ocean heat flux into the bottom of the ice layer F_w in units of W m^{-2} . Ice thickness is initially very thin, grows rapidly at first, and then reaches equilibrium thickness, which is very sensitive to the ocean flux. ($T_s = -30^\circ\text{C}$, other parameters as described in the text.)

Sea ice models used in state-of-the-art climate models are much more complex than the simple illustration given above. Important thermodynamic processes, such as the heat capacity of the sea ice and the brine incorporated in the ice have important effects on the amount and seasonality of sea ice and its response to climate forcing (Bitz and Lipscomb, 1999). Horizontal transport of sea ice is also important in many situations and plays a significant role in heat and salt transport in the high-latitude oceans. In the Arctic Ocean, the mean ice thickness is about 3–4 m, whereas in the Antarctic the average thickness is 1–2 m. The thinner Antarctic sea ice may be related to a greater supply of heat to the sea ice by ocean fluxes in the Antarctic. Also, more mechanical deformation of the ice in the closed basin of the Arctic Ocean may contribute to the greater average thickness there compared to the Antarctic sea ice, which is less constrained by shorelines and can simply spread equatorward until it melts (Fig. 11.5). Where sea ice is driven together by winds and current, pressure ridges can be formed where the ice thickness exceeds 10 m. As part of the same process, small openings in the ice (leads) or larger areas of open water (polynyas) can be produced. In these regions of open water, enhanced heat loss and ice formation occur in the season of ice growth, and more absorption of solar radiation occurs in the melting season. Around Antarctica, the formation of leads near the shoreline by the offshore advection of sea ice enhances the freezing rate of seawater, and the associated salt rejection is an important driver of bottom water formation around Antarctica.

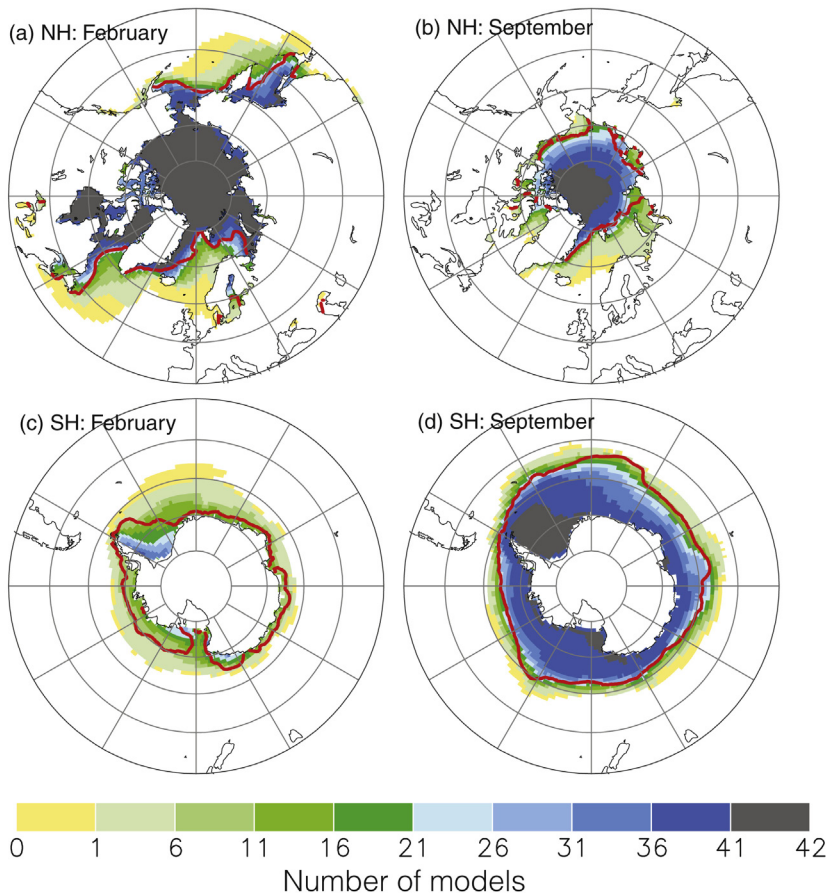


FIGURE 11.5 Sea ice distribution (1986–2005) in the Northern Hemisphere (a,b) and the Southern Hemisphere (c,d) for February (c) and September (d). AR5 baseline climate (1986–2005) simulated by 42 CMIP5 AOGCMs. Each model is represented with a single simulation. For each 1° × 1° longitude–latitude grid cell, the figure indicates the number of models for which at least 15% of the area is covered by sea ice. The observed 15% concentration boundaries (red lines) are based on the Hadley Centre Sea Ice and sea surface temperature (HadISST) data set (Rayner et al., 2003). Adapted from Pavlova et al., 2011. Figure and caption reproduced exactly from IPCC WG I Report Fig. 9.43, Flato et al. (2013).

11.7 VALIDATION OF CLIMATE MODEL SIMULATIONS

The simulations obtained with current climate models are in reasonable accord with observations of the present climate for a variety of key dynamic and thermodynamic climate variables (Flato et al., 2013). Models can produce most key features of the atmospheric general circulation

discussed in Chapter 6. Current models can reproduce the observed seasonal climatology of surface temperature to fairly high accuracy, with some exceptions over high topography or in regions of ocean upwelling in the tropics (Reichler and Kim, 2008). Accurate reproduction of observed surface temperatures over the equatorial oceans where the atmosphere and ocean are strongly coupled remains a challenge for climate models. Coupled atmosphere–ocean models simulate the observed ENSO cycle with varying degrees of fidelity (Guilyardi et al., 2009). The simulation of precipitation patterns is less good than temperature, with pattern correlations of 0.82 compared to 0.99 for surface temperature. The simulation of clouds remains a significant challenge for climate models. The simulation of the observed distribution of clouds by the model ensemble still has some biases and it is recognized that cloud feedback remains one of the primary uncertainties in modeling the climate response to greenhouse gas increases.

If the observed climate forcing by greenhouse gases, aerosols, volcanoes, and total solar irradiance are specified, then climate models can simulate the observed global mean surface warming and ocean heat content increases of the twentieth century. As far as we can tell from the observed climate record, models can do a reasonable job of simulating the year-to-year variability of Northern Hemisphere and global surface temperature variations, and many models currently also simulate the natural variability associated with El Niño.

This agreement is highly encouraging, but it does not by itself mean that climate models are capable of accurately predicting the response of climate to a natural or human-induced perturbation. The reason for skepticism is that a large number of adjustable constants are introduced in the parameterizations for sub-grid-scale phenomena and processes, and these parameters often cannot be determined on the basis of fundamental principles, but rather are set to values that give the most realistic-looking simulation of the current climate. For example, ocean models are very sensitive to the specification of sub-grid-scale mixing. Real confidence in the predictive capability of climate models can be gained by testing their simulations in great detail, so that the number of observational constraints is not too small compared to the number of independently specified parameters. It is also critically important to test their response to prescribed forcings for which the response is known. Examples of prescribed forcings are the annual and diurnal cycles of solar heating, the response to an event such as a major volcanic eruption, the response of the atmosphere to an observed SST anomaly, or the response of the climate model to the boundary conditions of an ice age (see Chapter 12). In this section, we will discuss what aspects of the climate system current models can simulate well and some aspects that remain problematical.

At the present time, many organizations in many countries have developed and operate climate models that simulate the coupling of the atmosphere, ocean, cryosphere, and land surface, and thus can be used to make projections of how the climate will respond to past and future changes of the climate system that may occur as a result of natural causes or intervention in the climate system by humans. A process for conducting common experiments and sharing simulation data has been organized under the auspices of the Climate Model Intercomparison Project (CMIP). At the time of this writing the results from CMIP5 are available (Taylor et al., 2012) and were used in the Intergovernmental Panel on Climate Change (IPCC) 5th Assessment (Stocker et al., 2013). To the extent that these models are independent, comparing them gives insight into our ability to model the climate system robustly and to what extent the predictions about future climate are robust.

An example of using model ensembles to evaluate our ability to simulate climate is given in Fig. 11.5, which shows the simulation of sea ice by CMIP5 models. The simulation of sea ice is a good and important test for climate models; since it involves both the ocean circulation and atmospheric circulation, surface ice feedback is very important for climate change projections, and the fate of sea ice is one of the important questions related to global warming. The red line shows the point where the satellite-observed sea ice concentration climatology is 15%, with latitudes poleward of this point generally having greater than 15% sea ice concentration. The color shading in the plot indicates how many models have at least 15% sea ice concentration at that point. In most cases, the red line falls where the color shading is between green and blue. This means that about half the models have more than 15% concentration and half have less. This is a good result since it means that the average of the models is probably about right. On the other hand, one can clearly see that some models have far too much sea ice and others have far to little. In general, taking the average of the models, the multimodel mean, is almost always better than picking a model at random, and for most purposes also better than picking the one model that seems to be best at whatever metric of success that you consider. The error of the multimodel mean of the seasonal distribution of sea ice is less than about 10%.

11.8 FEEDBACK STRENGTH AND SENSITIVITY ESTIMATES FROM CLIMATE MODELS

Global climate models can be used to estimate how various processes interact to determine the sensitivity of climate. In this section, we review some of the key results from using GCMs to assess climate sensitivity mechanisms. The basic concepts of forcing, feedback, and sensitivity

were introduced in Chapter 10. Model feedbacks and sensitivities can be assessed by attempting to simulate the observed record, or by imposing arbitrary idealized forcings on climate models and assessing their response. Climate forcings and temperature changes that have been so far observed are generally small, so a big arbitrary forcing often makes a more exciting experiment, but it is much more compelling to compare observed climate responses with observed forcings that the real climate system has actually experienced.

11.8.1 Water-Vapor Feedback

It is certain that water-vapor feedback exists and it is the strongest positive feedback, but since it is so strong, uncertainties in its magnitude are practically significant, especially since the strength of individual feedbacks magnify the effect of every other feedback. For example, if water-vapor feedback is stronger (or weaker), it is likely that it will warm more in response to a specified forcing, and the net effect of ice-albedo feedback will be greater (or less).

An observational test of water-vapor feedback in a climate model was made possible by the eruption of Mt. Pinatubo in June of 1991. Mt. Pinatubo was an explosive eruption containing large amounts of SO₂, so it made a significant aerosol cloud in the stratosphere that cooled the climate for several years. The surface cooling peaked at about 0.5 K about 18 months after the eruption. The response of the Earth radiation budget and the temperature and humidity profiles in the atmosphere to the Pinatubo eruption were well measured by global satellite observations. The absorbed solar radiation declined about 4 W m⁻² when the stratospheric aerosol cloud was at its maximum. The specific humidity of the atmosphere decreased by about 3%, in good agreement with the Clausius–Clapeyron relation indicating 7% per °C, assuming nearly constant relative humidity.

A schematic diagram of the responses of top-of-atmospheric radiation fluxes together with tropospheric temperature and column water vapor to a volcanic eruption is shown in Fig. 11.6. A little over a year after the eruption the absorbed shortwave radiation has decreased, owing to the reflection of sunlight by stratospheric aerosols. The shortwave response is delayed about a year because of the time it takes the released SO₂ gas to convert into sulfuric acid aerosols. The troposphere starts to cool in response to the reduction in solar heating, and the column water vapor decreases with the temperature in good accord with an assumption of fixed relative humidity. The OLR decreases as the planet cools, and because the aerosol cloud also absorbs some of the OLR and emits at a lower temperature. The cooling and drying persist longer than the stratospheric aerosol cloud because of the heat capacity of the ocean.

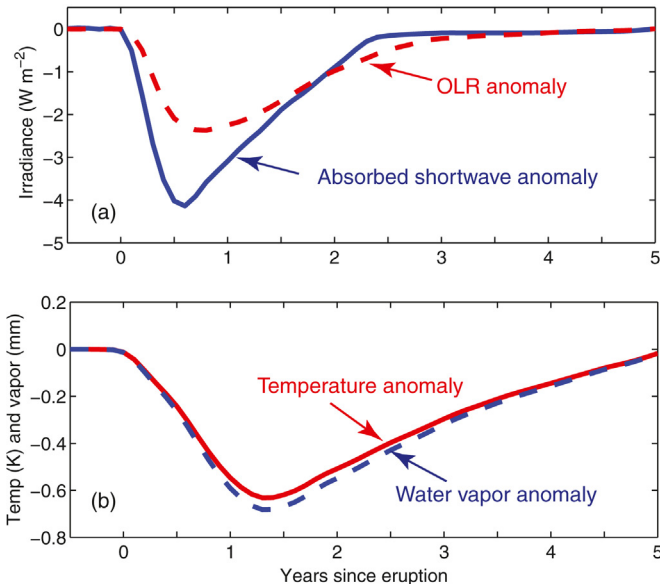


FIGURE 11.6 Schematic diagram of the observed anomalies of (a) absorbed shortwave and outgoing longwave radiation (OLR) and (b) tropospheric temperature and column water vapor to an explosive volcanic eruption that puts SO_2 into the stratosphere. Real data for the eruption of Pinatubo in 1991 is shown in Soden et al. (2002).

Soden et al. (2002) used a GCM to compute the response to the Pinatubo aerosols. The model produced the observed cooling and the observed reduction in tropospheric specific humidity. Using the model, they were able to show that the observed cooling is not obtained with the model unless the positive feedback associated with the specific humidity reduction is included. The experiment thus proved that the model could simulate the observed water vapor response and also that the positive water-vapor feedback of the magnitude simulated in the model was necessary to obtain the observed cooling. This and many other analyses of models and observations indicate that water-vapor feedback is strongly positive, as expected, and that GCMs can simulate it very well.

11.8.2 Planck and Water-Vapor Feedback in GCMs

Feedback processes in GCMs can be assessed using linear methods. The radiative transfer calculations performed by GCMs can be used to calculate the linear sensitivity of the top-of-atmosphere energy budget to changes of temperature and water vapor at any point in the atmosphere. Suppose that we have conducted a climate change experiment with a GCM and we want to assess the relative importance of Planck, water vapor, cloud, and surface albedo feedbacks. If we have applied some climate forcing dQ ,

then the temperature (T), water vapor (q), cloud (C), and surface albedo (α_s) changes must conspire to change the top of the atmosphere radiation balance by a compensating amount to achieve a new equilibrium for which $dR_{\text{net}} = dQ$. This change in radiation balance can be written,

$$dR_{\text{net}} \equiv \frac{\partial R_{\text{net}}}{\partial T} dT + \frac{\partial R_{\text{net}}}{\partial q} dq + \frac{\partial R_{\text{net}}}{\partial C} dC + \frac{\partial R_{\text{net}}}{\partial \alpha_s} d\alpha_s \quad (11.7)$$

Note that T , q , and C are functions of longitude, latitude, pressure, and time, whereas surface albedo is a function of longitude, latitude, and time, and $R_{\text{net}} = Q_{\text{abs}} - OLR$ has a solar and a terrestrial radiation component. It is also helpful to note that (11.7) can be written as,

$$dR_{\text{net}} \equiv dR_{\text{net}}^T + dR_{\text{net}}^q + dR_{\text{net}}^C + dR_{\text{net}}^{\alpha_s} \quad (11.8)$$

so that one can explicitly think of each term as contributing part of the change in the radiation balance that results from warming.

The partial derivatives can be calculated by changing T , q , C and α_s by standard amounts. Then these partial derivatives can be multiplied by the actual changes from a climate change experiment (dT , dq , dC , $d\alpha_s$) to obtain the feedbacks. The sensitivities in (11.7) were first calculated and used by Soden et al. (2008) who termed them radiative kernels, so we introduce a kernel notation for each feedback variable, rewriting (11.7) as,

$$dR_{\text{net}} \equiv K_T dT + K_q dq + K_C dC + K_{\alpha_s} d\alpha_s \quad (11.9)$$

K_T translates the changes of temperature at every pressure, latitude, longitude, and season into a change in the top-of-atmosphere radiation balance at every latitude, longitude, and season. K_q does this for humidity changes, K_C for clouds, and K_{α_s} for surface albedo.

The feedbacks can be referenced to the global mean surface temperature change $d\bar{T}_s$, which will facilitate comparing and combining feedbacks from different models. We can thus also write (11.7) as

$$dR_{\text{net}} \equiv (\lambda_T^{-1} + \lambda_q^{-1} + \lambda_C^{-1} + \lambda_{\alpha_s}^{-1}) d\bar{T}_s \quad (11.10)$$

Here these feedbacks are defined as

$$\lambda_x^{-1} = \frac{\partial R_{\text{net}}}{\partial x} \frac{dx}{d\bar{T}_s} \quad (11.11)$$

where $x = T$, q , α_s , and C represent the influence on feedback of temperature, humidity, surface albedo, and cloudiness.

Fig. 11.7 shows the kernels, the changes in climate parameters and the feedbacks for temperature and water vapor averaged for a suite of 28 GCMs from the Fifth Coupled Model Intercomparison Project (CMIP5, Taylor et al., 2012) averaged over season and longitude. The changes and

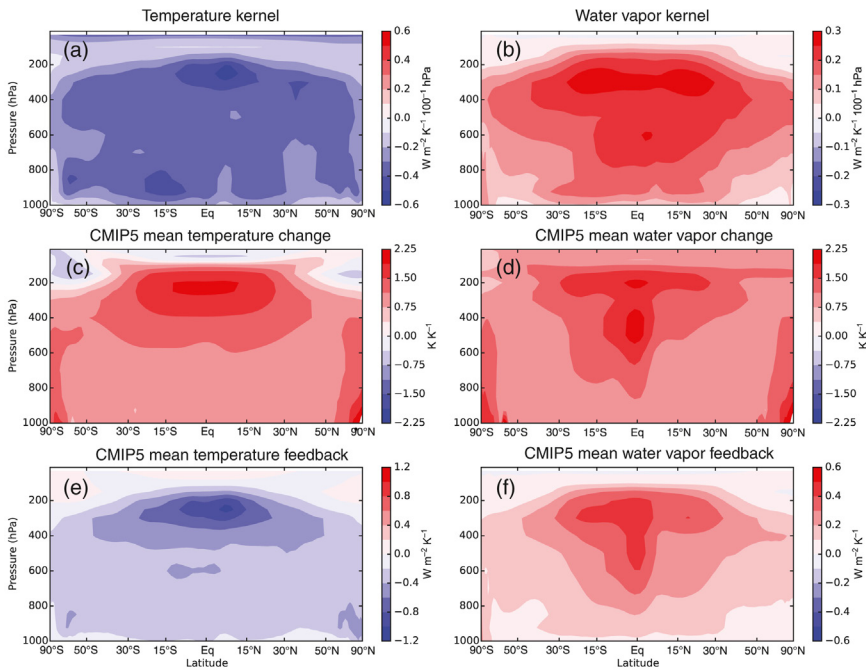


FIGURE 11.7 Kernels, changes, and feedbacks for temperature (Planck feedback) and water vapor (water-vapor feedback) averaged over season, longitude and a suite of CMIP5 models. Note that the abscissa in these plots is scaled by sine of latitude, so that the relative importance of latitude zones for the global mean is properly represented. The area between the equator and 30°N is the same as the area from 30°N to 90°N. *Figure courtesy M.D. Zelinka.*

feedbacks are normalized to a global mean temperature increase of 1 K to remove variations associated with the sensitivity of individual models and allow the unbiased construction of a multimodel mean. The effects of average model cloudiness are included in the computation of the kernels. Clouds partially screen the effects of water vapor, temperature, and albedo changes that occur below them. For water vapor, the increment used to compute the kernels is the change in specific humidity associated with a 1 K increase in temperature if the relative humidity is kept constant. So both the temperature and water vapor kernels are normalized for 1 K temperature increase and can be directly compared.

Figure 11.7a shows the sensitivity of R_{net} to temperature changes in 100 hPa thick layers, averaged over longitude and season. R_{net} decreases for temperature increases at all locations, since the Planck emission increases with temperature. The sensitivity is a little less very near the surface, and a little more just below the tropical tropopause and at the top of the boundary layer in the southern subtropics. These are regions where the transmission is changing with height and the OLR is more sensitive to temperature (Fig. 3.9). Figure 11.7b shows the same thing for water vapor.

R_{net} is most sensitive to water vapor changes in the upper troposphere, since this is the region where emission to space from water vapor is greatest. Increases in water vapor move the emission upward to lower temperatures and thus trap more longwave radiation, so the R_{net} sensitivity is everywhere positive. R_{net} is less sensitive to water vapor changes lower in the atmosphere, since a blanket of water vapor and clouds lies above these lower levels, and this mutes the effect of changes at lower levels on radiative fluxes at the top of the atmosphere.

Figure 11.7c shows the average temperature change, normalized so that the global mean surface warming is 1 K. Models generally warm the upper tropical troposphere and the polar regions about twice as much as the global mean. The water vapor increase shows a similar amplification in these two regions, as well as an enhancement along the equator where the models on average generate more intense convection in a warmed Earth (Fig. 11.7d). Figure 11.7e,f show the product of the upper two panels. Temperature feedback is negative everywhere in the troposphere, with stronger negative feedback in the upper tropical troposphere, not only because it warms more there but also because the kernel is larger there. The stratosphere cools in response to CO₂ increases, but the contribution of this to total feedback is fairly modest. Since the coordinates are proportional to area and mass, the total feedback can be estimated from visual averaging. The water-vapor feedback is positive and concentrated in the upper tropical troposphere (Fig. 7.11f). Note that the enhanced warming in the upper tropical troposphere causes enhanced negative feedback, but this is largely offset by increases in the positive feedback caused by the water vapor increase. This is an expression of the cancellation of lapse-rate feedback by water-vapor feedback discussed in relation to Fig. 10.6.

11.8.3 Cloud Feedback and Forcing Adjustment

Cloud feedback in climate models can also be estimated. It is of interest to know the relative contributions of cloud fractional area, cloud top height and cloud optical depth. These feedbacks can be estimated if these cloud properties are saved when the model computations are performed. It is useful to use an '*instrument simulator*', which takes the model variables and calculates the signals that an instrument on an Earth-orbiting satellite would measure, if that instrument were orbiting above the model. These simulated cloud observations can then be used both to test the model against observations and to assess the feedbacks using "*cloud kernels*" (Zelinka et al., 2012a,b). Such experiments with a simulator of the measurements from the International Satellite Cloud Climatology Project (ISCCP, Rossow and Schiffer, 1999) were done as part of the Cloud Feedback Model Intercomparison Project (CFMIP).

When the climate is forced by the introduction of additional greenhouse gases, such as a doubling of CO₂, the CO₂ changes the radiative heating rates in the atmosphere, which has an almost immediate effect on the clouds, since cloud-producing convection acts to balance the radiative cooling of the atmosphere (Fig. 3.18). Because the surface temperature may not have reacted yet to the CO₂ increase, owing to the heat capacity of the ocean, the effects of these fast-response cloud changes can be isolated in models and are usually assigned to the forcing, rather than to the feedback. One way to study these effects is to double or quadruple the CO₂ instantaneously, then try to measure the direct effect of the CO₂ increase on the clouds before the climate warms up very much (Zelinka et al., 2013). Such efforts show a relatively strong fast response of clouds to CO₂ before the climate begins to warm. Cloud fractional area, cloud top height, and cloud optical depth all decrease in response to a CO₂ increase, such that the cloud adjustment produces a net increase in the radiation balance, which adds to the direct warming effect of CO₂.

One can write the change in the radiation balance due to cloud changes, dR_C as an initial adjustment F_C , plus a part that depends linearly on the global mean surface temperature change, dT_s , and thus measures the cloud feedback λ_C^{-1} .

$$dR_C = F_C + \lambda_C^{-1} dT_s \quad (11.6)$$

The cloud adjustment to forcing and the cloud feedback can be estimated with a model by applying an instantaneous forcing, such as $4 \times \text{CO}_2$ or a 2% increase in TSI and then recording the change in the radiation balance caused by cloud changes and the surface temperature as the climate warms in response to the climate forcing (Gregory and Webb, 2008). It is apparent that the adjustment will be different for greenhouse gas increases and TSI changes. For a CO₂ increase, the atmospheric cooling is suppressed and for TSI the surface heating is enhanced, giving very different initial cloud responses. It is found that, although the fast response and the adjustment to forcing are different for CO₂ and TSI forcing, the feedbacks are very similar. This similarity of the estimated feedback strength for very different forcings is another good argument for assigning the fast, prewarming, adjustments of clouds to the forcing and including only the cloud changes that respond to temperature change in the calculation of cloud feedback. A drawback of this approach is that it buries some of the uncertainty associated with clouds in the forcing, which can otherwise be calculated very precisely if the temperature, water vapor, and clouds are assumed fixed. We can call the forcing that is adjusted for rapid responses of the stratosphere and clouds the *effective forcing*. An estimate of the effective climate forcing from doubling the CO₂ in current models is $3.5 \pm 0.5 \text{ W m}^{-2}$.

After this initial adjustment, the temperature begins to increase and cloud feedback can occur. Figure 11.8 shows the changes in cloud

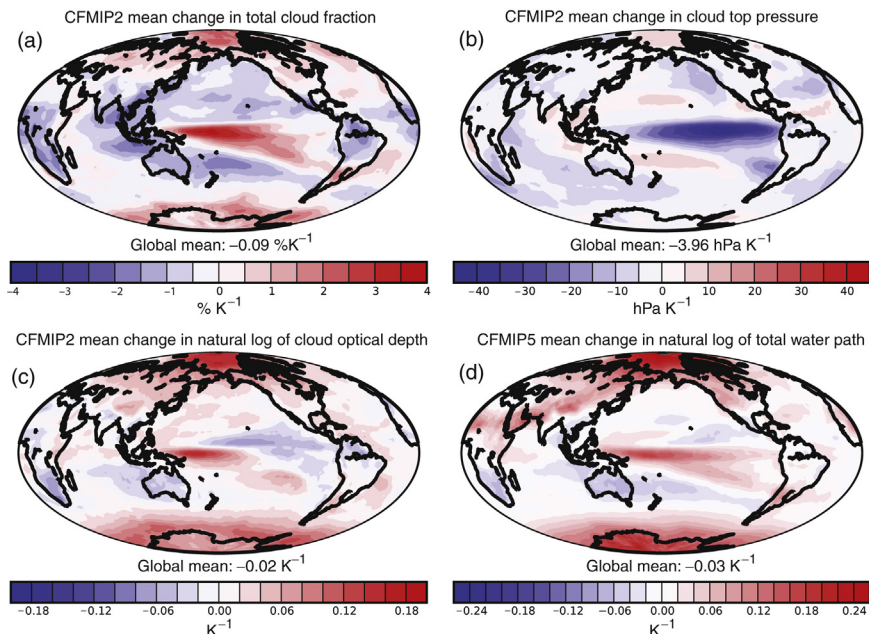


FIGURE 11.8 Change in cloud properties in response to warming resulting from $4 \times \text{CO}_2$ forcing from the multimodel mean of CFMIP2 abrupt $4 \times \text{CO}_2$ experiment. (a) Cloud fractional area, (b) cloud top pressure, (c) optical depth, and (d) total cloud water path. Changes are normalized for 1 K; global mean temperature increases. Courtesy of M.D. Zelinka.

fractional area, cloud top pressure, cloud optical depth, and cloud total water path for the CFMIP2 multimodel mean. Models show a redistribution of cloud fraction with warming, with increases in the Central Pacific and in high latitudes, and decreases elsewhere. The tropical changes are mostly related with the tendency of CMIP5 models to warm more in the eastern equatorial Pacific Ocean than elsewhere, giving an El Niño-like response. In the subtropics, enhanced entrainment of dry air and less radiative loss from cloud tops may be the cause of a general reduction in low cloud fraction. Cloud tops move upward and to lower pressures with warming (Fig. 11.8b). This is related to the increase in water vapor and increased efficiency of clear sky radiative cooling at higher altitudes in a warmed Earth, and with the greater amount of moist static energy in surface air. High clouds generally move upward with the expansion of the troposphere. Cloud optical depth and total cloud water path increase at high latitudes and in convective regions of the tropics, but decrease slightly elsewhere. This is in part related not only to the increase in water vapor with warming but also to the conversion of cloud ice to cloud water as the models warm. Cloud water persists in the atmosphere longer than cloud ice and is more reflective per unit mass, owing to the smaller particle radius of liquid water clouds.

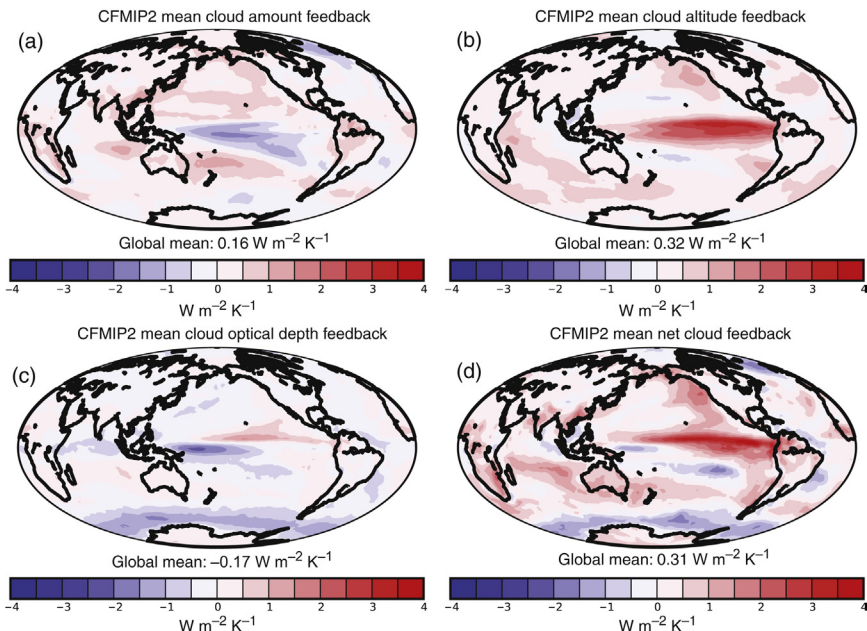


FIGURE 11.9 Cloud feedbacks from the multimodel mean of CFMIP2 abrupt $4 \times \text{CO}_2$ experiment. (a) Cloud fractional area, (b) cloud top pressure, (c) optical depth, and (d) net cloud feedback. Changes are normalized for 1 K; global mean temperature increases. Courtesy of M.D. Zelinka.

Figure 11.9 shows the feedbacks associated with the cloud property changes shown in Fig. 11.8. Reductions in cloud fraction give a net positive feedback in most regions because the clouds have a negative impact on the radiation balance. Much of the cloud reduction is in low clouds over the oceans, which have a particularly strong negative impact on the radiation balance (Hartmann et al., 1992). High cloud altitudes increase nearly everywhere and this gives a strong positive cloud altitude feedback. Optical depth feedback in the models is also positive over the subtropics, but strongly negative in other regions, which dominate to give a net negative feedback from cloud optical depth increases. The brightening of clouds over the Southern Ocean is particularly strong. Warming causes the microphysics in these models to convert ice clouds to water clouds, which increases the liquid water path and cloud reflection. Net cloud feedback in the models is overall fairly strongly positive, but has strong spatial gradients. It is very positive in the tropical Pacific, but quite negative over the Southern Ocean. These gradients in net feedback give rise to circulation responses. Despite the fact that the meridional gradient of surface temperature weakens, the meridional gradients of net top-of-atmosphere radiative heating and moist static energy both increase, and so does the meridional energy transport.

11.8.4 Ice–Albedo Feedback

Climate models simulate land snow cover and sea ice on a seasonal basis, and so the effect of ice–albedo feedback is included in climate models. Models designed for projecting the climate a century or two into the future generally assume that the permanent ice sheets over Greenland and Antarctica are fixed in place, although the effects of snow cover and surface melting on the albedo of ice sheets can be included. The surface albedo kernel and the magnitude of ice–albedo feedback in CMIP5 models are shown in Fig. 11.10. The impact of surface albedo changes on the energy balance would be greatest in cloud-free regions of the tropical oceans,

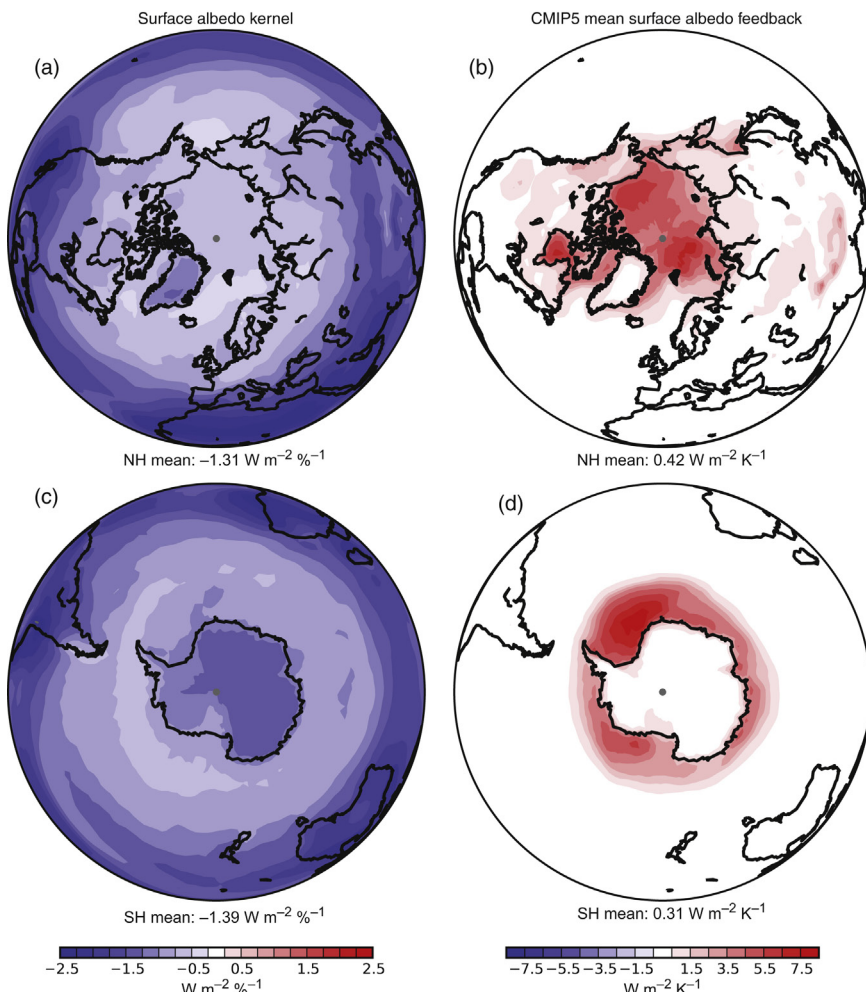


FIGURE 11.10 Surface albedo kernel (a,c) and surface albedo feedback estimate (b,d) from CMIP5 models abrupt $4 \times \text{CO}_2$ experiments. Courtesy of M.D. Zelinka.

since the insolation is large and the current planetary albedo is relatively low there. In high latitudes where the insolation is less and the cloud cover is greater, the sensitivity to surface albedo changes is less, but this is the region where ice and snow are present and can contract or expand with warming or cooling. The surface albedo feedback is mostly concentrated over the high latitude or high altitude land areas of the Northern Hemisphere and over the regions of sea ice in the Arctic and Antarctic Oceans.

11.8.5 Summary of Model Energetic Feedbacks

By considering an ensemble of models and adjusting the forcing for the fast response to CO₂, one can assess the magnitude of the key climate feedbacks and their uncertainties. Figure 11.11 shows feedbacks and uncertainties from a suite of CMIP5 model simulations. The uncertainties are estimated as twice the standard deviation of the model-to-model variation, which gives a general notion of which feedbacks are well quantified and which are still uncertain. A two standard deviation variation also approximates the spread of the individual model assessments of feedback from least negative to most negative. The Planck feedback is the top-of-atmosphere radiation balance change induced by a uniform increase in temperature of 1 K everywhere. This gives a strong negative feedback

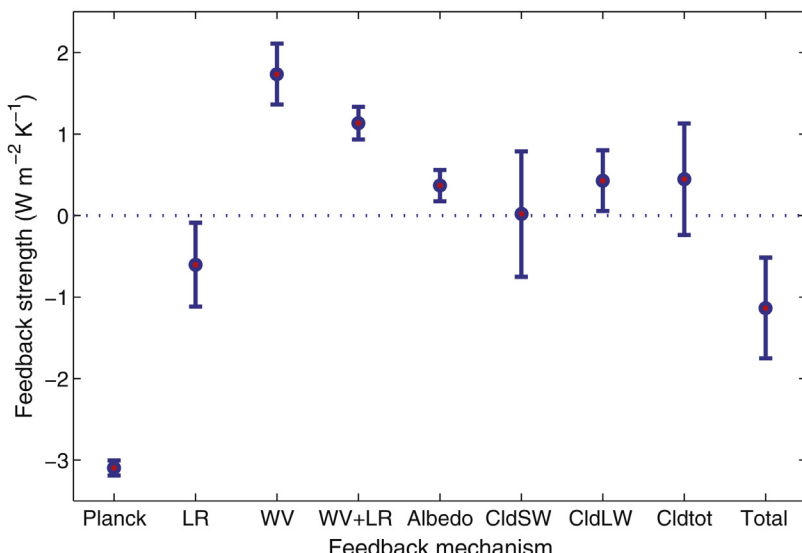


FIGURE 11.11 Strengths and uncertainties of various feedbacks from a suite of CMIP5 models. Uncertainties are estimated as ± 2 times the standard deviation among the 28 models in the ensemble. LR, Lapse rate; WV, water vapor; Cld, Cloud; SW, shortwave; LW, longwave; Tot, LW + SW; Total is sum of all feedbacks. Data Courtesy of Mark Zelinka.

of about $-3.1 \text{ W m}^{-2} \text{ K}^{-1}$ with little uncertainty, corresponding to the sensitivity of blackbody emission for a temperature of about 240 K.

Lapse-rate feedback is the feedback that results from the structure of the temperature change, especially the reduction of lapse rate in the tropics, which is a negative feedback. Water-vapor feedback is the change in radiation balance caused by the increase of water vapor with temperature. Note that when lapse rate and water-vapor feedback are combined, the uncertainty is reduced. This was explained in Fig. 10.6. Surface-albedo feedback is related to the melting of surface ice with warming. It is relatively small and positive. Longwave, shortwave, and total cloud feedback are highly uncertain, with total feedback slightly positive. When all the feedbacks are combined, the best estimate of the total feedback is about $-1.2 \pm 0.6 \text{ W m}^{-2} \text{ K}^{-1}$, but it is uncertain by about $\pm 50\%$. Most of this uncertainty is associated with cloud feedbacks. The total feedback controls the magnitude of the warming associated with forcing such as a doubling of CO₂. Note that to obtain the global mean temperature response, the forcing is divided by the feedback (11.4). If the adjusted forcing for a doubling of CO₂ is 3.5 W m⁻², then the uncertainty in total feedback gives predicted equilibrium warming from doubling of CO₂ that falls in the range from 2 K to 5.8 K with a best estimate of 2.9 K. Narrowing the uncertainty in feedback is thus key to good estimates of how much impact will result from doubling or quadrupling CO₂.

11.8.6 Hydrologic Cycle Feedback

When surface temperature changes, one of the most significant responses is that the saturation water vapor increases about 7% K⁻¹ of warming. This fundamental physical effect has multiple implications for climate change, including the cycling of water between the surface and atmosphere. In Section 5.5, we showed that potential evaporation should increase rapidly with warming, meaning that land areas will dry out more quickly after rain, and evaporation over the ocean will increase in a warmed earth. Since water vapor decreases exponentially with decreasing temperature, the decrease of specific humidity with altitude also becomes stronger with warming. Thus if air is pushed upward, more precipitation will result per degree of adiabatic cooling in a warmer climate. We might then expect the hydrologic cycle to get much stronger in a warmed Earth, with more evaporation and more rainfall. However, we saw in Chapter 6 that the atmospheric energy balance constrains the evaporation rate to the rate at which the atmosphere can cool radiatively, at least in the global mean (Pendergrass and Hartmann, 2014). Therefore, the atmosphere has to adjust to the fact that when air is moved upward it releases more latent heat, but that the rate at which radiative cooling of the atmosphere increases with warming is much less than the Clausius–Clapeyron rate of 7% K⁻¹, at least in part because water-vapor feedback constrains the cooling to space. One way for the atmosphere to solve this

dilemma is for the circulation to slow down, with less overturning so that the upward mass flux of water vapor is reduced. Another possible solution is to confine the upward motion to a smaller area, so that cloud-free dry zones that can more efficiently radiate to space are expanded. Over the tropical oceans, the models can reduce evaporation by reducing wind speed or increasing relative humidity near the surface as the climate warms.

Let's begin by looking at how the zonal mean relative humidity in models responds to warming. Figure 11.12 shows the zonal and annual mean relative humidity for the present climate and the change in relative humidity with warming in a suite of CMIP5 models. The modeled relative humidity is generally a good depiction of the observed relative humidity shown in Fig. 10.4. With warming, the troposphere deepens, so that relative humidity

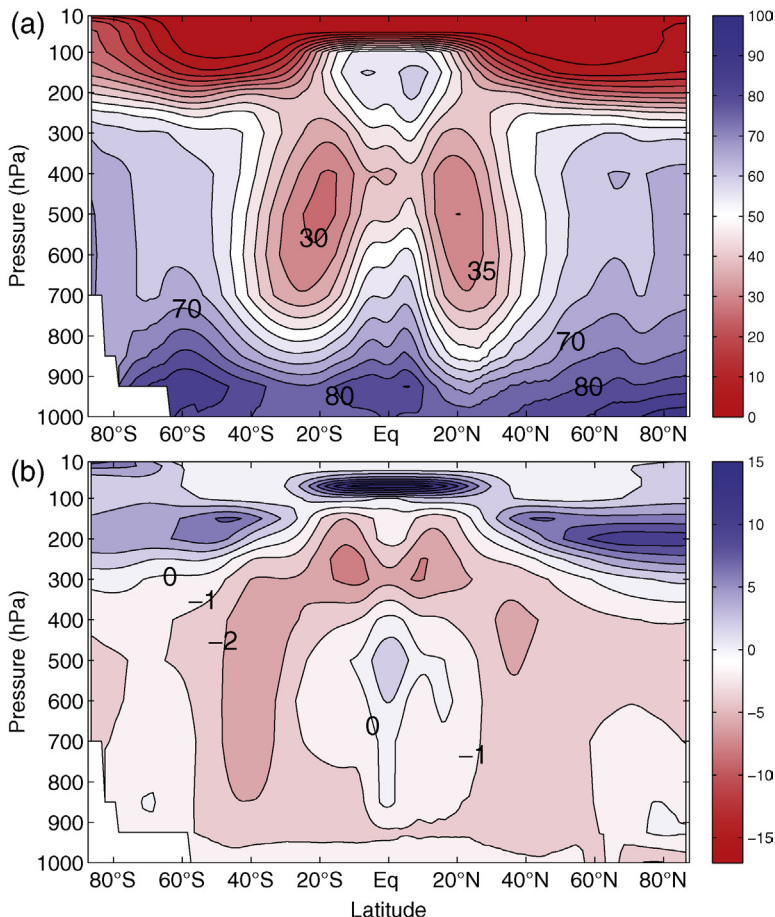


FIGURE 11.12 Zonal cross-section of percent relative humidity of (a) the historical climate of CMIP5 models and (b) the change in the relative humidity from the historical to the RCP 8.5 scenario for 2080–2100. Contour interval is 5% in (a) and 1% in (b).

increases in the vicinity of the tropopause and decreases below, except near the equator in the middle and lower troposphere where it moistens. The reduction in relative humidity is stronger around 40°N and 40°S , especially in the Southern Hemisphere. This enhanced drying in the subtropics and lower middle latitudes is associated with the poleward expansion of the dry zones that are the most prominent features of the climatology, apart from the extreme aridity of the stratosphere. These changes occur in association with an expansion of the Hadley cell and a poleward movement of the extratropical jets. The jet movement is particularly evident in the Southern Hemisphere, where the eddy-driven jet is a more dominant feature and responds fairly strongly to climate change by moving poleward (Fig. 11.13b). The troposphere expands upward to lower pressures in a warmed climate,

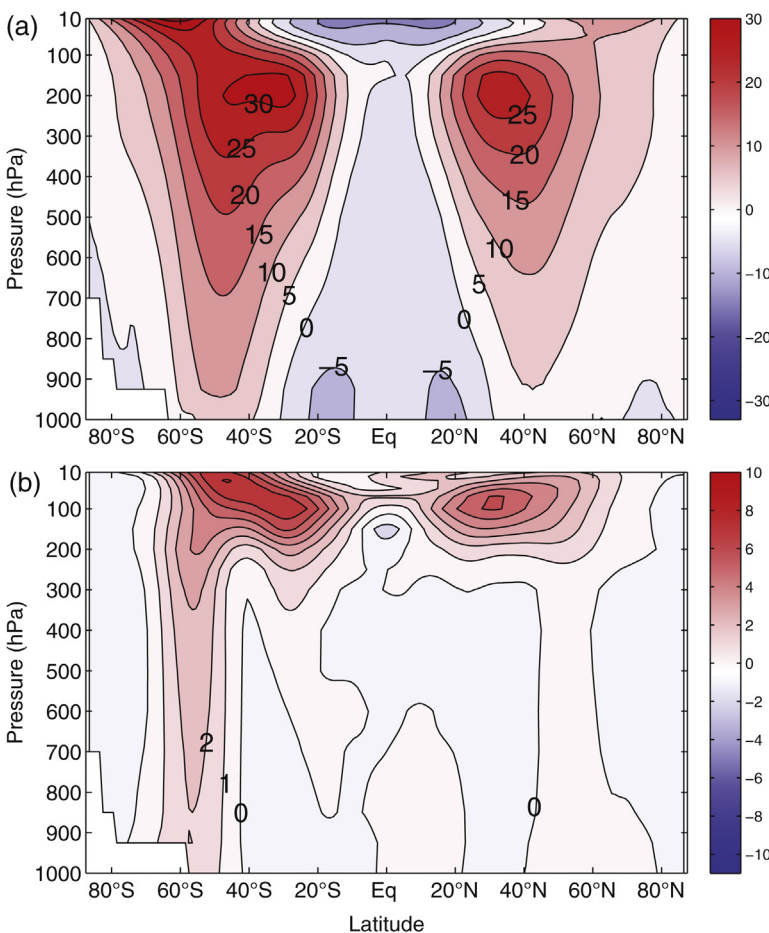


FIGURE 11.13 Zonal cross-section of zonal mean wind of (a) the historical control simulation from CMIP5, and (b) the change from the historical simulation to the 2080–2100 RCP 8.5 simulation. Contour interval is 5 m s^{-1} in (a) and 1 m s^{-1} in (b).

and so the winds in the upper troposphere increase as the subtropical and midlatitude jets move upward. The poleward jet movement in the Southern Hemisphere is aided by the cloud feedback, which intensifies the gradient in radiative heating by reducing the absorbed solar radiation in high latitudes and increasing it in lower latitudes (Fig. 11.9).

The net effect of the expansion of the subtropical dry zone and the wet-gets-wetter, dry-gets-drier paradigm is reflected in simulations of the changed surface hydrology in response to global warming (Fig. 11.14). Precipitation increases in the tropical Pacific and high latitudes and decreases elsewhere. Evaporation increases nearly everywhere. Relative humidity of surface air increases over the oceans, but decreases over land. The increase over the oceans is consistent with the constraint that the global evaporation cannot increase at the Clausius–Clapeyron rate like the saturation humidity, but is constrained by the rate at which the atmosphere can dispose of the latent heating by radiative emission. As previously mentioned models can reduce evaporation by increasing surface relative humidity a little, which will suppress the evaporation rate (4.32). Figure 11.14 clearly shows that most models do increase surface relative humidity over the ocean, even though the evaporation goes up with the saturation vapor pressure. E–P has a very strong zonal structure with increases in the subtropics and decreases elsewhere. This is consistent with the strengthening of the contrast in the hydrologic cycle that we expect from basic considerations. The implications of this for land areas is indicated by the modeled changes in runoff and soil moisture in Fig. 11.14. CMIP5 models fairly consistently predict drying of subtropical land areas and wetting of other regions. Regions that seem particularly likely to dry out are the American Southwest, the Mediterranean, northern South America, and southern Africa.

11.9 COUPLED ATMOSPHERE–OCEAN PROCESSES AND THE THERMOHALINE CIRCULATION

Models of the ocean in coupled AOGCMs can simulate the response of the ocean to climate change. In the case of warming, the upper ocean warms quickly, except in those regions where vertical mixing is efficient, such as the North Atlantic and the Southern Ocean surrounding Antarctica, where the surface warming is delayed. The penetration of the heating to deeper levels of the ocean proceeds more slowly, since it takes deep water formation in polar latitudes as much as a thousand years to replace the abyssal ocean water. As the heating of the surface water proceeds the ocean becomes more stable and deep water formation may slow. Also, the addition of freshwater in high latitudes owing to the increased precipitation there can slow down the meridional overturning cells. The different local responses of the ocean to warming may impart important structure to the warming. The key examples of this are the slowed warming in the North

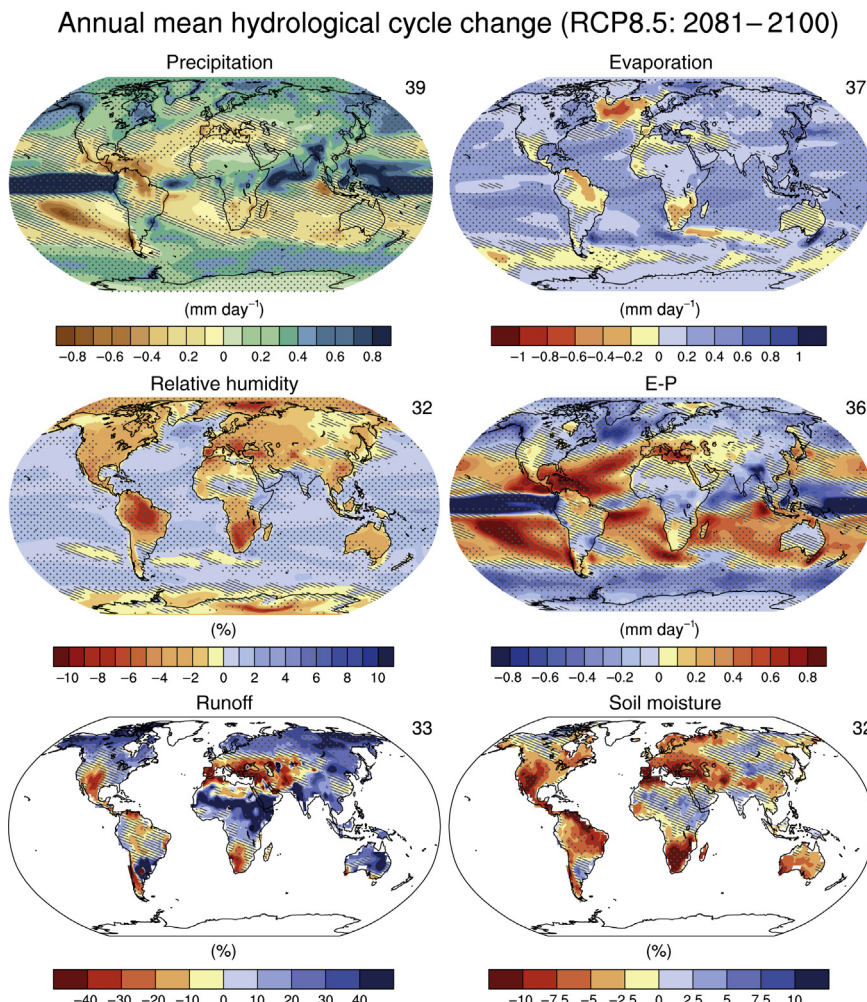


FIGURE 11.14 Annual mean changes in precipitation (P), evaporation (E), relative humidity, E–P, runoff and soil moisture for 2081–2100 relative to 1986–2005 under the Representative Concentration Pathway 8.5 (RCP8.5). The number of Coupled Model Intercomparison Project Phase 5 (CMIP5) models to calculate the multimodel mean is indicated in the upper right corner of each panel. Hatching indicates regions where the multimodel mean change is less than one standard deviation of internal variability. Stippling indicates regions where the multimodel mean change is greater than two standard deviations of internal variability and where 90% of models agree on the sign of change. Figure and caption reproduced exactly from IPCC WG I Report Technical Summary Fig. TFE.1, Fig. 3, Stocker et al. (2013).

Atlantic and the Southern Ocean associated with the deep overturning circulation, and the greater warming of the eastern equatorial Pacific compared to the tropics as a whole (Fig. 11.15). Most, but not all models have these features. Other features of the land-sea contrast of projected transient

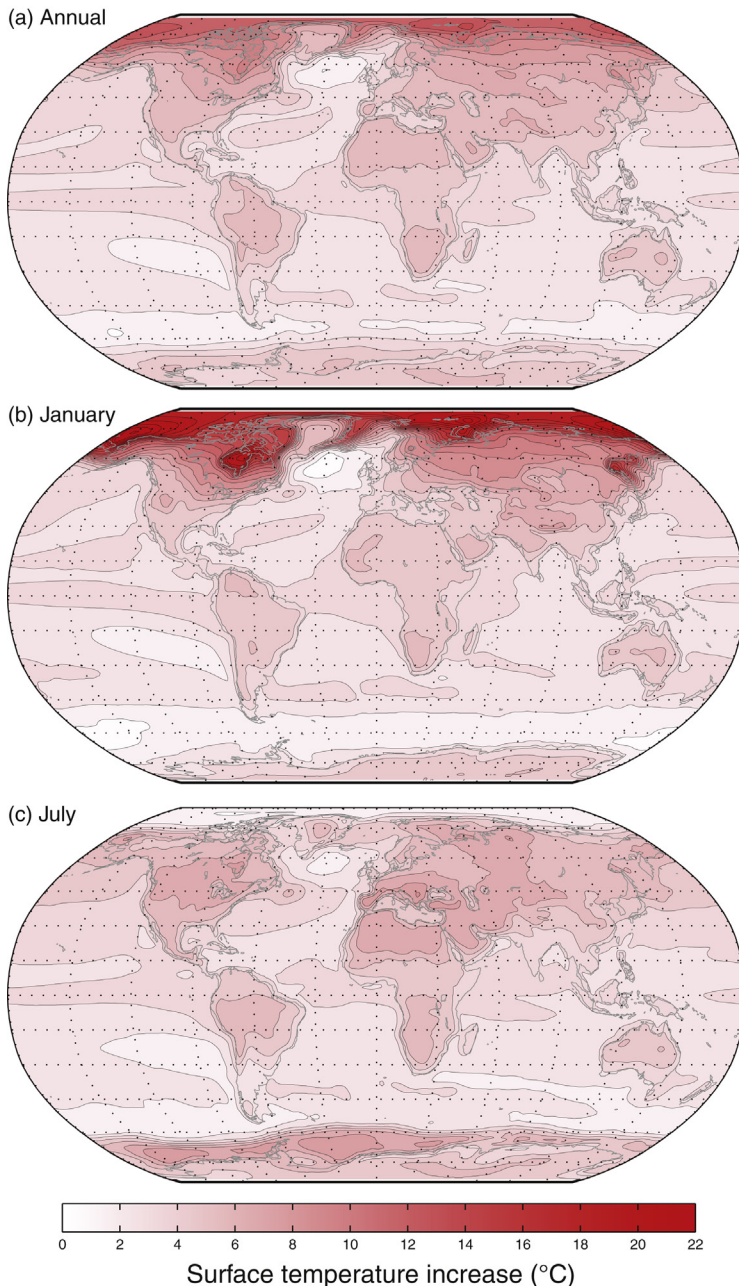


FIGURE 11.15 Surface temperature increases between RCP8.5 2081–2100 and historical simulation from CMIP5 multimodel mean. Contour interval is 1°C.

warming at the end of the twenty-first century are greater warming over land than ocean and greater warming in winter than summer in high latitudes. In regions with sea ice, the surface temperature cannot increase much in summer, when the ice melts a little, but still may be present, and if the ice is completely removed, then the large ocean heat capacity keeps it from warming as much in these regions. If the ice melts out in summer, then the ocean takes in much more stored heat, the sea ice is thinner, and the wintertime surface temperatures increase a lot in a warmed Earth. This is especially true in the Arctic in January, but is also true in regions of Antarctic sea ice in winter (July). In the Arctic the warming is smaller than average in summer and larger than average in winter.

The wet-gets-wetter, dry-gets drier paradigm for the hydrological cycle also has a reflection in ocean salinity. Ocean surface salinity is an integrator of the hydrological cycle, with saltier surface waters where $E-P > 0$ and fresher waters where $E-P < 0$. In most models, the Atlantic gets saltier in tropical and subtropical latitudes, but fresher in the far North Atlantic as the climate warms in twenty-first century simulations. Since the north Atlantic also warms a little and the density near freezing is most sensitive to salinity, deep water formation in the North Atlantic becomes less likely, and the Atlantic meridional overturning circulation slows down in most models as the climate warms. Analysis of trends in salinity data suggest that the trend toward a saltier Atlantic and greater contrast between salty and fresh regions of the surface ocean has already begun (Durack et al., 2012).

EXERCISES

1. Suppose that the air temperature above the Arctic Ocean is -30°C and the water temperature is -2°C . Solve for the sensible heat flux to the atmosphere if the bulk aerodynamic formula for heat flux (4.26) applies with surface pressure 10^5 Pa , $C_{\text{DH}} = 10^{-3}$, and $U_r = 5 \text{ m s}^{-1}$. Assume a steady state with no heat storage and ignore radiative and latent heat fluxes. Consider three cases: (a) no sea ice, (b) 1 m of sea ice, and (c) 3 m of sea ice. Solve for the temperature of the surface in those cases with sea ice. Use (11.3) with $k_i = 2 \text{ W m}^{-1} \text{ K}^{-1}$ to solve for the flux through the ice.
2. Repeat problem 1 for the case of 1 m of sea ice with 10 cm of snow on top. Use $k_s = 0.3 \text{ W m}^{-1} \text{ K}^{-1}$.
3. Calculate the surface temperature and sea ice thickness in equilibrium under the following conditions: polar darkness, air temperature -40°C , surface pressure 10^5 Pa , $C_{\text{DH}} = 10^{-3}$, $U_r = 5 \text{ m s}^{-1}$, and $k_i = 2 \text{ W m}^{-1} \text{ K}^{-1}$. The downward longwave flux is 100 W m^{-2} , and the surface has unit longwave emissivity. Consider cases where the ocean supplies heat to the base of the ice at the rate of (a) 10 W m^{-2} and (b) 20 W m^{-2} . Hint: Use the energy balance at the surface and at the base of the ice and linearize

the Stefan–Boltzmann emission about the air temperature. Ignore latent cooling.

4. What would be the equilibrium sea ice thickness for the two cases of problem 3 if the sea ice were covered by 20 cm of snow with $k_s = 0.3 \text{ W m}^{-1} \text{ K}^{-1}$?
 5. Look in the tropical Pacific at the cloud changes in Fig. 11.8 and at the precipitation changes in Fig. 11.14. Explain how these are consistent with each other.
 6. Compare the relative humidity changes in Fig. 11.12 with the zonal mean wind changes in Fig. 11.13. Explain how these are consistent with the general circulation of the atmosphere described in Chapter 6, and the modes of natural variability described in Fig. 8.4.
 7. In Fig. 11.15, the January warming is much greater over Hudson Bay than over the surrounding land regions of North American. Can you explain this?
-